Deep tissue imaging with multiphoton microscopy in the short-wavelength infrared windows

Konstantinos Bourdakos, Lin Xu, Anna Crisford, Duanyang Xu, Ibrahim Abughazaleh, et al.

SPIE.

Deep tissue imaging with Multiphoton microscopy in the Short-wavelength Infrared windows

Konstantinos N. Bourdakos[a,c*], Lin Xu[b], Anna Crisford[c], Duanyang Xu[b], Ibrahim Abughazaleh[b], Peter B. Johnson[a,c], Hiroki Cook[c], Panuwat Srisamran[b], Richard O.C. Oreffo[d], David J. Richardson[b], and Sumeet Mahajan[a,c]

[a]School of Chemistry, Faculty of Engineering and Physical Sciences, University of Southampton, UK, [b]Optoelectronics Research Centre University of Southampton, UK, [c]Institute for Life Sciences, University of Southampton, Southampton, UK, [d]Centre for Human Development, Stem Cells and Regeneration, Institute of Developmental Sciences, University of Southampton, UK

Abstract

Multiphoton microscopies are an invaluable tool in biomedical imaging given their inherent capabilities for label free imaging, optical sectioning, chemical and structural specificity. They comprise various types of Coherent Raman microscopies (CR), such as Coherent Anti-Stokes Raman Scattering (CARS), Stimulated Raman Loss (SRL) or Stimulated Raman Gain, different kinds of Harmonic Generation imaging (HG) such as Second and Third Harmonic Generation (SHG and THG respectively), and Multiphoton Autofluorescence imaging (MA) such as Two and Three Photon Excited Autofluorescence (TPEAF and ThPEAF respectively). Despite their significant advantages, multiphoton microscopies, comparably to all other types of optical microscopies, exhibit limited penetration depth in tissue due to absorption and scattering.

In this work we explore the advantages of multiphoton microscopies in hard and soft deep tissue imaging when using excitation wavelengths in the range of Short-Wavelength Infrared (SWIR) windows which occur between 1000 nm and 2500 nm. These spectral windows have notable merits including longer attenuation lengths and none or very low signal absorption observed for almost all kinds of multiphoton microscopy. We show results of using excitations in the SWIR windows, generated by standard as well as novel sources, such as a thulium fibre laser, in different types of multiphoton microscopy on a variety of hard and soft tissue samples (bone, cartilage and other tissue types) and demonstrate the advantages of using excitations in this wavelength range, including longer penetration depth and high resolution for deep tissue imaging.

Keywords: Multiphoton microscopy, Third Harmonic Generation, Short – Wavelength Infrared windows

1. INTRODUCTION

Over the last few decades the field of optical microscopy has been completely transformed due to the deployment of new imaging concepts and the rapid advancement of laser and computer technologies. One of the new imaging concepts that has seen tremendous development is that of multiphoton microscopy which comprises a suite of versatile imaging methods based on the principles of nonlinear optics. Methods such as Coherent Raman[1,2,3], Harmonic Generation[4,5,6,7] and Multiphoton Excited Autofluorescence[8,9,10,11], constitute a multitude of nonlinear optical imaging techniques that can recover three dimensional chemical and structural information from biological specimens.

In particular Harmonic Generation microscopy consists of mainly two techniques which are the Second and Third Harmonic Generation (SHG and THG respectively) imaging. Both of these modalities are coherent, label free, and have optical sectioning capabilities[12,13]. More specifically SHG has been used in imaging non-centrosymmetric structures either extracellular such as collagen fibrils[4], or intracellular such as cytoskeletal microtubules related to mitotic spindles and axons[12]. SHG has been used as a neuroimaging modality to investigate neurodegenerative disorders including Alzheimer's disease and glaucoma in which damage or breakdown of axonal microtubules is involved[14, 15]. It has also been deployed

---

* K.N.Bourdakos@soton.ac.uk

in diseases and conditions such as pulmonary fibrosis in which disruption, alteration or damage of collagen fibrils is implicated[16].

On the other hand, THG has proved extremely powerful in the detection of interfaces and inhomogeneities in cells and tissue [17]. THG enables image acquisition without photobleaching and, in addition allows quantitative image analysis[18]. In contrast to second harmonic generation THG can be applied to any structure independently of their symmetries[19]. THG microscopy has been applied in the imaging of cellular membranes, lipid droplets, calcified bone[19], breast cancer tissue[18], brain tissue[20].

To date, most of the THG imaging has been performed using excitation wavelengths[17,18,19] between 1000 and 1350 nm, also known as NIR II optical window[21]. However the range (1550 – 1850 nm) which is known[21,22] as NIR III optical window has significant advantages regarding deep tissue imaging, such as longer attenuation length[20,21,22] and none or very low THG signal absorption from tissue as the latter appears at longer wavelengths[21]. However, biomedical imaging is very little explored in this spectral range due to a sparsity of laser light sources at these wavelengths[23]. The available laser sources for this wavelength range are the standard Optical Parametric Oscillators or Amplifiers[23] (OPO and OPA respectively) which are expensive, complex, require high maintenance and a dedicated optical lab and have a large footprint. Alternatively, the method of Raman Soliton self-frequency shift can be exploited for converting 1.5 μm femtosecond laser pulses, inside a photonic crystal fiber, to generate wavelengths in the NIR III range. Although cheaper than the OPO or OPA systems, this method suffers from low conversion efficiency and poor energy and wavelength stability as it is very sensitive to the coupling of the initial laser pulses in the photonic crystal fiber[24,25].

In this work we perform concurrent THG and SHG imaging by using non – standard wavelengths in the NIR III and NIR II optical windows respectively. For THG imaging we have deployed a novel Thulium Fiber Laser. We explore the performance of these imaging methods regarding their axial scanning capabilities, and we observe large penetration depths on two different types of bone samples.

2. METHODS

For the purpose of THG imaging in the NIR III optical window we have used as a light source a novel Thulium Fiber laser (Figure 1). A detailed description and performance analysis have been given elsewhere[26] and here only a very brief description of this light source will be presented. The Thulium fiber laser consists of the following parts: a fiber laser cavity, a stretcher, a 1st fiber amplifier, a 2nd fiber amplifier and a compressor. The fiber laser cavity has a length of a Thulium Doped Fiber (TDF) as the gain medium which is pumped by a laser diode (LD) at 1560 nm through a wavelength division multiplexer (WDM). In order to ensure a unidirectional oscillation in the cavity a semiconductor saturable absorber mirror (SESAM) was attached at the fiber end of a a polarization dependent circulator (PD circulator). A length of a dispersion compensation fiber (DCF) has been added in order to compensate for the anomalous dispersion in the cavity resulting in a net normal dispersion which is required for the dissipative soliton mode – locking operation. Two polarization controllers (PC) are used to control the polarization state of the intra – cavity pulses. The laser output is extracted through a 50% output coupler (OC) and delivered through an isolator (ISO) to a stretcher. The pulses are positively chirped in the stretcher to an appropriate pulse width for chirped pulse amplification. After the stretcher the pulses enter the 1st fiber amplifier which is comprised by a length of TDF pumped by an Erbium doped fiber laser (EDFL) through a WDM. After this stage and through an isolator the pulses enter the 2nd fiber amplifier which consists of the same kind of parts as the 1st one but has different fiber parameters. At the output of this amplification stage the output beam is collimated and through an isolator is delivered to a compressor consisted of two gratings and a roof mirror. The output of the compressor consists of 416 fs pulses at 1840 nm with a repetition rate of 16 MHz and a maximum average power around 1 W.

The SHG imaging is performed by using a commercial Ytterbium fiber laser (Emerald Engine, APE Berlin), which outputs 2 ps pulses at 1031 nm with a repetition rate of 80 MHz. The available maximum average power for SHG imaging was around 1 W.

The two beams are set colinear through a short pass dichroic beam splitter (Figure 2) for concurrent imaging. A custom-built inverted microscope based on a Nikon Ti Eclipse frame, which is equipped with a pair of galvanometer mirrors for laser scanning is used for imaging. The two colinear beams are coupled into the scanner, and after passing through a pair

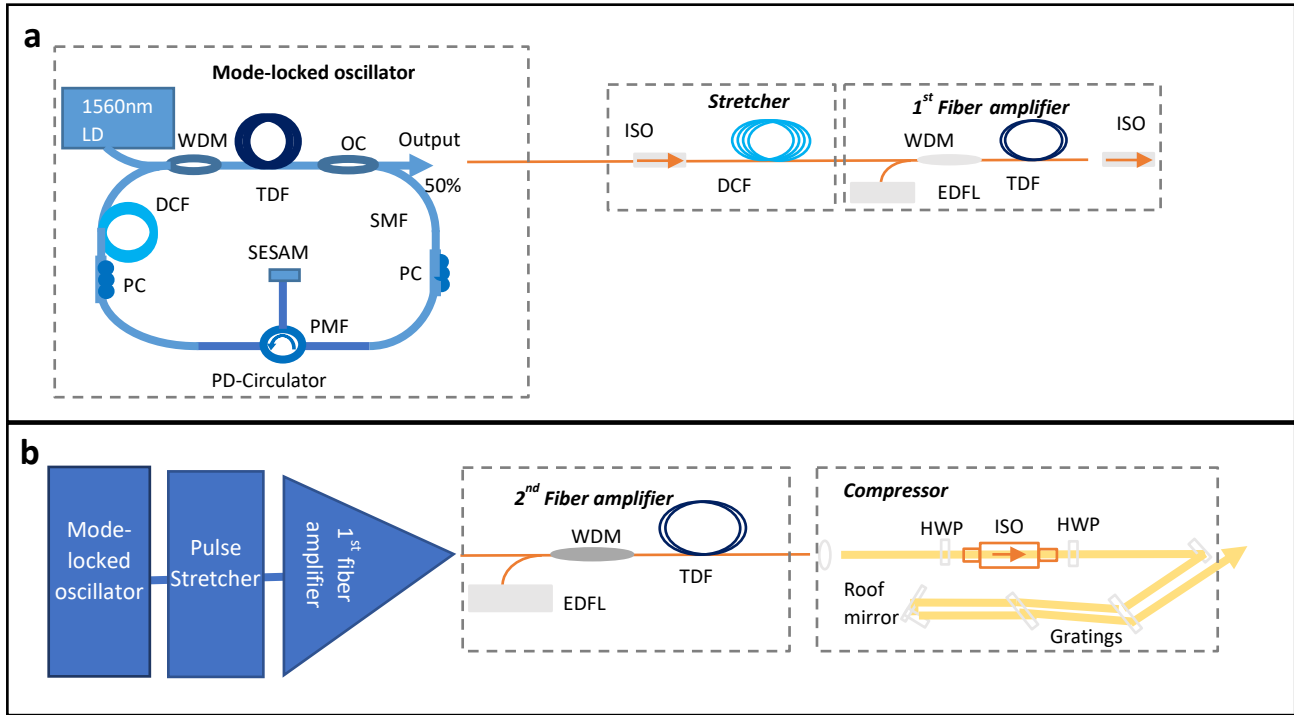of lenses (scan lens and tube lens) they are reflected by a short-pass

Figure 1 Schematic of the Thulium Fibre Laser. a) the mode-locked oscillator, stretcher and 1st fiber amplifier, b) the 2nd fiber amplifier and the compressor. Abbreviations: WDM: wavelength-division multiplexer; TDF: thulium doped fiber; OC: output coupler; SMF: single mode fiber; PC: polarization controller; PD-Circulator: polarization dependant circulator; DCF: dispersion compensate fiber; LD: laser diode; PMF: polarization maintaining fiber, ISO: isolator, EDFL: erbium dopped fiber laser, HWP: half – wave plate.

dichroic (excitation dichroic) beam splitter and focused on the samples through an infinity corrected objective. The SHG and THG signals are collected in the back-scattering (epi-detection) geometry from the same objective and delivered ultimately to a long pass dichroic beam splitter in the detection branch where they are spectrally separated (Figure 2). Then the two separated signals are delivered through the appropriate narrow band-pass filters to two photomultiplier tube (PMT) detectors. The scanner and the detectors are interfaced with a DAQ-PCI6110 to a desktop computer. The laser scanning and the acquisition are controlled with Scanimage 6.1 (Vidrio Technologies). All the image acquisitions were performed with a 20x objective lens with a numerical aperture (NA) of 0.75. The pixel resolution of each image was 512x512 which, for the objective and the scanning settings that we have used, corresponded to a field of view of 250 μm x 250 μm, while the pixel dwell time was 16 μs. Finally, all of the acquired images were processed with Fiji (ImageJ).

3. RESULTS AND DISCUSSION

Two types of samples were imaged via the means of THG and SHG microscopy. The one sample is a cortical section of an antler and the images are presented in Figure 3. As the purpose of this image acquisition was to demonstrate the performance of the THG and SHG in the NIR II and NIR III optical windows there would be no attempt of thorough anatomical identification of the features present in the acquired images, but only a brief description of the images and in

some cases a simple evaluation of the possible nature of the observed features. Only representative images at different depths are presented to illustrate the variation with THG and SHG in the sample with depth.
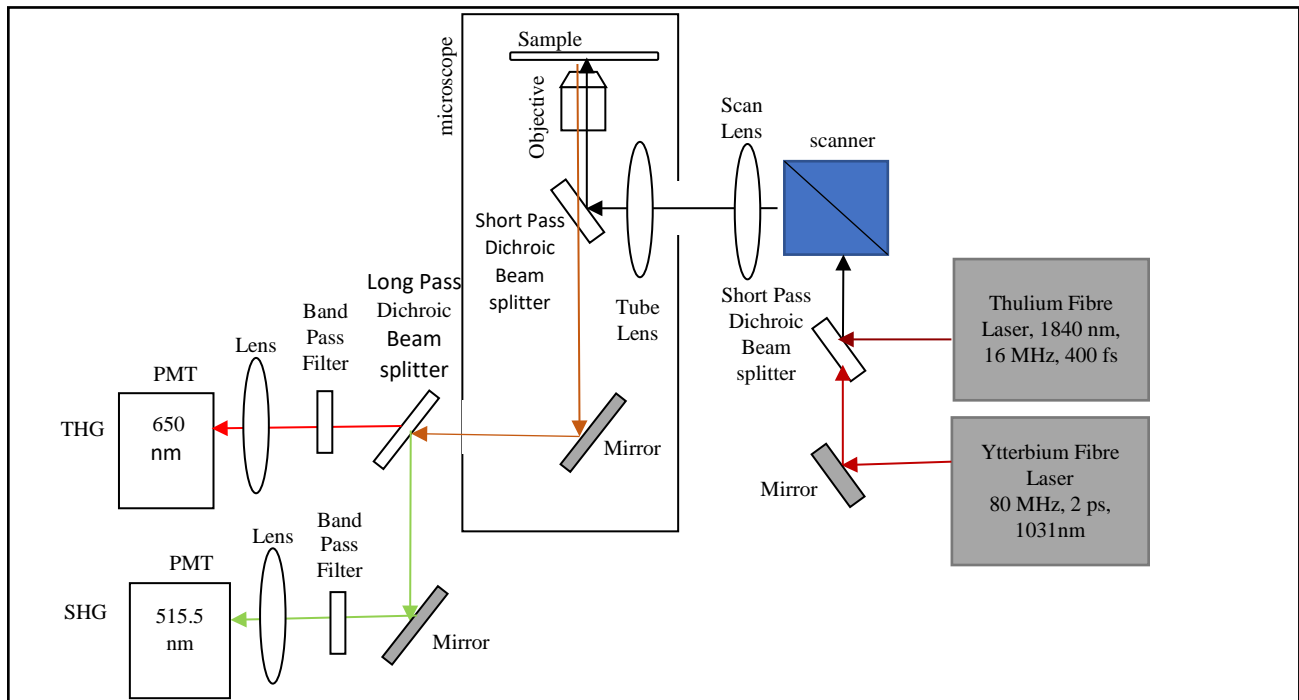

Figure 2 Schematic of the imaging setup.

In Figure 3 THG and SHG images of a cortical antler section are shown at depths of 0, 10, 20, and 70 μm. The THG image at 0 μm shows a lamellar structure which seems to persist for a few microns below the surface. On the other hand, the respective SHG images show some fibrillar formations that exhibit long straight and parallel segments, and it is very likely that they are collagen fibers. At a depth of 10 μm the texture of the THG image changes completely showing fibrillar formations which are different than ones observed in the SHG images as they seem to be thinner and shorter with relatively short straight parts. In both cases (THG and SHG images) the observed fibres appear to be well embedded in the bone matrix. Similar features at higher depths down to 70 μm for the THG images and 40 μm for the SHG images. Below these depths all features faded rapidly and there was not anything distinguishable.

The second sample that was imaged was a thin slice of human rib cage normal bone biopsy section (Amsbio, USA). THG and SHG images of this sample are shown in Figure 4 at depths of 0, 10, 20, and 30 μm. At the surface (0 μm) a granular structure in the bone marrow compartment and a part of the surrounding inorganic matrix deposit can be distinguished with high contrast in the corresponding THG image. The respective SHG image shows the collagen matrix while it exhibits a complete lack of signal in the bone marrow compartment. Similar features can be observed in the respective THG and SHG images at 10 μm depth. At this depth an empty area close to the centre of the bone marrow compartment can be observed in the THG image, while collagen fibers can be distinguished in the SHG image. Further at 20 μm depth the THG image demonstrates the soft tissue compartment where various features such as vascular canals and blood vessels can be seen. In addition, potentially erythrocytes, large dots in the blood vessels can be distinguished. Surrounding the bone marrow compartment, the bone mineral matrix can be seen in the same image. Similarly in the SHG image for this depth, the surrounding collagen matrix can be observed. Finally at the depth of 30 μm another texture of the area around the bone marrow compartment is revealed in the THG image while the SHG image is similar to that of the previous depth and appears to have faded. The reduction in the image contrast is observed for both channels (THG and SHG) down to 40 μm depth after which no distinguishable features could be observed.
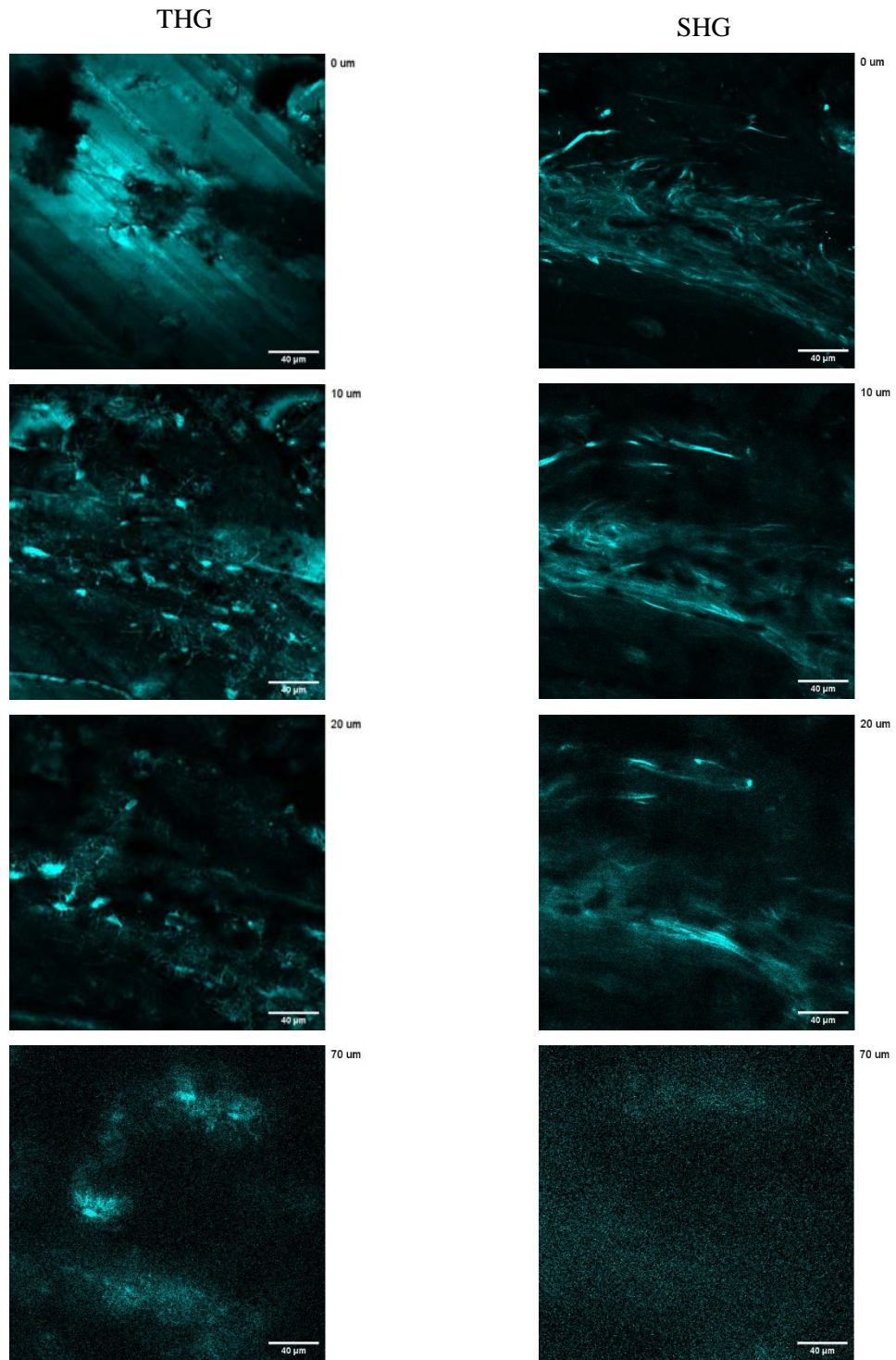
THG

SHG

Figure 3 THG left and SHG right images of an antler cortical section at depths of 0, 10, 20 and 70 μm.
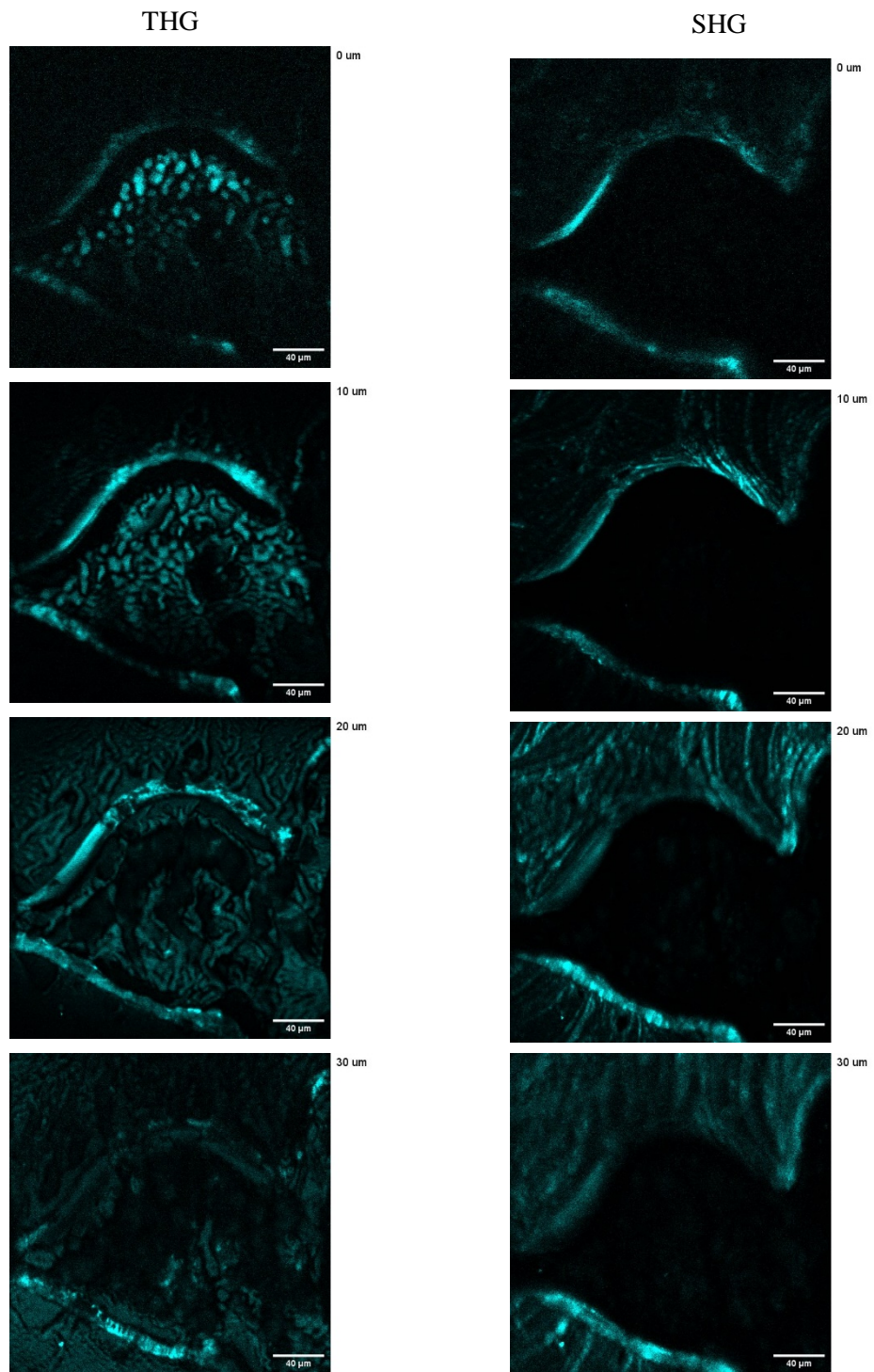
THG   SHG

Figure 4 THG left and SHG right images of a section of human bone in depths of 0, 10, 20, and 30 μm.

4. CONCLUSIONS

In conclusion we have demonstrated that the NIR III optical window can be exploited for deep tissue THG imaging with high contrast and resolution. A novel Thulium laser was deployed successfully as a light source for THG imaging. SHG imaging using a commercial light source was concurrently performed with THG imaging. Penetration depths of approximately 70 μm on antler and 40 μm on a human rib cage bone sample were achieved for THG microscopy under the current imaging conditions

REFERENCES

[1] Cheng, J-X.; Xie, XS. Coherent Raman Scattering Microscopy. London: CRC; 2012.

[2] Prince, R. C., Potma, E. O. "Coherent Raman scattering microscopy: capable solution in search of a larger audience," J. Biomed. Opt. 26(6) 060601 (2021).

[3] Zhang, C., Zhang, D., Cheng, J. X., "Coherent Raman Scattering Microscopy in Biology and Medicine," Annu. Rev. Biomed. Eng. 17, 415-45, (2015).

[4] Pavone, F.S., & Campagnola, P.J. (Eds.), Second Harmonic Generation Imaging (1st ed.), CRC Press, (2013).

[5] Campagnola, P., "Second harmonic generation imaging microscopy: applications to diseases diagnostics," Anal. Chem. 83(9), 3224-31, (2011).

[6] Weigelin, B., Bakker, G.J., Friedl, P., "Third harmonic generation microscopy of cells and tissue organization," J. Cell Sci., 129 (2), 245–255, (2016).

[7] Squier, J. A., Müller, M., Brakenhoff, G. J., Wilson, K. R., "Third harmonic generation microscopy," Opt. Express 3, 315-324 (1998).

[8] Kretschmer, S., Pieper, M., Hüttmann, G. et al., "Autofluorescence multiphoton microscopy for visualization of tissue morphology and cellular dynamics in murine and human airways," Lab Invest 96, 918–931 (2016).

[9] Li, L. Z., Masek, M., Wang, T., Xu, H. N., Nioka, S., Baur, J. A., Ragan, T. M., "Two-Photon Autofluorescence Imaging of Fixed Tissues: Feasibility and Potential Values for Biomedical Applications," Adv. Exp. Med. Biol., 1232, 375-381, (2020)

[10]Li, D., Zheng, W., and Qu, J. Y., "Two-photon autofluorescence microscopy of multicolor excitation," Opt. Lett. 34, 202-204 (2009)

[11]Durr, N. J., Ben-Yakar, Ad., Weisspfennig, C. T., Holfeld, B. A., "Maximum imaging depth of two-photon autofluorescence microscopy in epithelial tissues," J. Biomed. Opt. 16(2), 026008 (2011)

[12] Lim H., "Harmonic Generation Microscopy 2.0: New Tricks Empowering Intravital Imaging for Neuroscience." Front. Mol. Biosci. 6:99, (2019)

[13] Campagnola, P., Loew, L., "Second-harmonic imaging microscopy for visualizing biomolecular arrays in cells, tissues and organisms." Nat Biotechnol 21, 1356–1360 (2003).

[14] Zempel, H., Thies, E., Mandelkow, E., and Mandelkow, E., M., "Abeta oligomers cause localized Ca(2+) elevation, missorting of endogenous Tau into dendrites, Tau phosphorylation, and destruction of microtubules and spines." J.Neurosci. 30, 11938–11950, (2010).

[15] Huang, X., R., Knighton, R., W., and Cavuoto, L., N., "Microtubule contribution to the reflectance of the retinal nerve fiber layer." Invest. Ophthalmol. Vis. Sci. 47, 5363–5367, (2006).

[16] Jones, M., G., Andriotis, O., G., et al., "Nanoscale dysregulation of collagen structure-function disrupts mechano-homeostasis and mediates pulmonary fibrosis" eLife 7:e36354, (2018).

[17] Genthial, R., Beaurepaire, E., Schanne-Klein, MC. *et al.* Label-free imaging of bone multiscale porosity and interfaces using third-harmonic generation microscopy. *Sci Rep* **7,** 3419 (2017).

[18] Gavgiotaki, E., Filippidis, G., Tsafas, V. *et al.* Third Harmonic Generation microscopy distinguishes malignant cell grade in human breast tissue biopsies. *Sci Rep* **10,** 11055 (2020)

[19] Bettina Weigelin, Gert-Jan Bakker, Peter Friedl. Third harmonic generation microscopy of cells and tissue organization. J Cell Sci **129**, 245, (2016).

[20] Horton, N., Wang, K., Kobat, D. *et al. In vivo* three-photon microscopy of subcortical structures within an intact mouse brain. *Nature Photon* **7,** 205–209 (2013).

[21] Yusuke Murakami, Minori Masaki, Shinichi Miyazaki, Ryosuke Oketani, Yu Hayashi, Masashi Yanagisawa, Sakiko Honjoh, and Hideaki Kano, "Spectroscopic second and third harmonic generation microscopy using a femtosecond laser source in the third near-infrared (NIR-III) optical window," Biomed. Opt. Express **13**, 694 (2022).

[22] Laura A. Sordillo, Yang Pu, Sebastião Pratavieira, Yury Budansky, Robert R. Alfano, "Deep optical imaging of tissue using the second and third near-infrared spectral windows," J. Biomed. Opt. 19(5) 056004 (7 May 2014)

[23] Castro-Olvera, G., Morselli, S., Gacci, M., Serni, S., Liaci, A., Nicoletti, R., Loza-Alvarez, P., "Multimodal SWIR Laser Imaging for Assessment and Detection of Urothelial Carcinomas" , in Sordillo, L. A., Sordillo, P., P., eds "Short-Wavelength Infrared Windows for Biomedical Applications", SPIE Press, Bellingham, Washington, USA, (2022)

[24] Li, B., Wu, C., Wang, M., Charan, K., and Xu, C., "An adaptive excitation source for high-speed multiphoton microscopy," 17(2), 163-166 (2020).

[25] Wang, K., Pan, Y., Tong, S., Liang, H., and Qiu, P., "Deep-skin multiphoton microscopy of lymphatic vessels excited at the 1700-nm window in vivo," Biomed. Opt. Express. 12(10), 6474-6484 (2021).

[26] Xu, L., Xu, D., Bourdakos, K., N., Johnson, P., B., Crisford, A., Abughazaleh, I., Srisamran, P., Fu, Q., Mahajan, S., and Richardson, D., J., "1840-nm femtosecond thulium fiber laser system for label-free third-harmonic generation microscopy," in Conference on Lasers and Electro-Optics, Technical Digest Series (Optica Publishing Group, 2022), paper JM4E.5.